Int. J. Engng Sci. Vol. 26, No. 2, pp. 183–192, 1988
Printed in Great Britain

0020-7225/88 $3.00 + 0.00
Pergamon Press plc

STEADY STATE DEFORMATIONS OF A RIGID PERFECTLY PLASTIC ROD STRIKING A RIGID CAVITY

R. C. BATRA and PEI-RONG LIN

Deparment of Engineering Mechanics, University of Missouri-Rolla, Rolla, MO 65401-0249, U.S.A.

Abstract—The axisymmetric steady state deformations of an infinite cylindrical rod made of a rigid/perfectly plastic material and striking a known cavity in a rigid target are analyzed by the finite element method. The contact between the deforming rod and the target surface is assumed to be smooth. It is found that the axial force experienced by the rod depends strongly upon the square of its speed. Results computed and presented graphically include the velocity field in the deforming region, the dependence of the shape of the upset head of the striker upon its speed, and the distribution of normal tractions upon the cavity wall.

INTRODUCTION

Penetration of metal targets by projectiles is influenced by such variables as material properties, impact velocity, projectile shape, target support position, and relative dimensions of the target and the projectile. Recently, emphasis has been placed on kinetic energy penetrators, which for terminal ballistic purposes may be considered as long metal rods traveling at high speeds. Wright [1], in his survey article on long rod penetrators, ellucidated vividly some of the problems with the existing penetration models. In another extensive review article, Backman and Goldsmith [2] discussed superbly the work done in penetration mechanics until 1977. Jonas and Zukas [3] reviewed various analytical methods for the study of kinetic energy projectile-armor interaction at ordance velocities and placed particular emphasis on three-dimensional numerical simulation of perforation. Anderson and Bodner [4] have recently reviewed the status of the ballistic impact modeling. A penetration model that is not too difficult to use has been proposed by Ravid and Bodner [5]. They studied the penetration problem by presuming a kinematically admissible flow field in the target and found the unknown parameters by utilizing an upper bound theorem of plasticity modified to include dynamics effects.

In an attempt to shed some light on questions raised by Wright [1], Batra and Wright [6] recently studied an idealized penetration problem that simulates the following situation. Suppose that the penetrator is in the intermediate stages of penetration so that the active target/penetrator interface is at least one or two penetrator diameters away from either target face, and the remaining penetrator is much longer than several diameters and is still traveling at a speed close to its striking velocity. This situation has been idealized as follows. It is assumed that the rod is semi-infinite in length, the target is infinite with a semi-infinite hole, the rate of penetration and all flow fields are steady as seen from the nose of the penetrator, and that no shear stress can be transmitted across the target/penetrator interface. This last assumption is justified on the grounds that a thin layer of material at the interface either melts or is severely degraded by adiabatic shear. These idealizations make it possible to decompose the penetration problem into two parts in which either a rigid rod penetrates a deformable target or a deformable rod is upset at the bottom of a hole in a rigid target. Of course, in the combined case the contour of the hole is unknown, but if it can be chosen so that normal tractions match in the two cases along the entire boundary between penetrator and target, then the complete solution is known irrespective of the relative motion at the boundary. Even without matching the normal tractions, it would seem that valuable qualitative information about the flow field and distribution of stresses can be gained if the chosen contour is reasonably close to those that are found in experiments.

Whereas Batra and Wright [6] studied the problem of the deforming target and a rigid penetrator, we analyze herein the companion problem of a deformable, semi-infinite and cylindrical penetrator striking a known semi-infinite cavity in an infinite and rigid target. Only the axisymmetric and steady state problem in which the penetrator material is rigid/perfectly plastic has been studied. This problem is more challenging than the one studied earlier by Batra and Wright [6] because of the presence in it of free surfaces whose shapes are not known *a priori*. We hope that the kinematic and stress fields found in this study would help in devising and/or checking results from simpler engineering theories of penetration.

FORMULATION OF THE PROBLEM

We describe the deformations of the cylindrical rod upset at the bottom of a semi-infinite cavity in an infinite rigid target with respect to a cylindrical coordinate system with origin at the center of the hole and z-axis pointing into the rod. Equations governing the steady state axisymmetric deformations of the rod are

$$\operatorname{div} \mathbf{v} = 0, \tag{1}$$

$$\operatorname{div} \boldsymbol{\sigma} = \rho \dot{\mathbf{v}}, \tag{2.1}$$

$$= \rho(\mathbf{v} \cdot \operatorname{grad})\mathbf{v}. \tag{2.2}$$

Here $\mathbf{v}$ is the velocity of a rod particle, ρ is the mass density and $\boldsymbol{\sigma}$ is the Cauchy stress tensor. Equation (1) implies that the deformations of the rod are isochoric, and eqn (2) expresses the balance of linear momentum. The operators grad and div signify the gradient and divergence operators on fields defined in the present configuration. We neglect the elastic deformations of the rod and assume that it is made of a homogeneous and isotropic material that obeys the Von-Mises yield criterion and the associated flow rule. Thus we take the following constitutive relation for $\boldsymbol{\sigma}$, e.g. see Prager and Hodge [7].

$$\boldsymbol{\sigma} = -p\mathbf{1} + \frac{\sigma_0}{\sqrt{3}\,I}\mathbf{D}, \tag{3}$$

$$\mathbf{D} = (\operatorname{grad} \mathbf{v} + (\operatorname{grad} \mathbf{v})^T)/2, \tag{4}$$

$$I^2 = \frac{1}{2} \operatorname{tr} \mathbf{D}^2. \tag{5}$$

In eqn (3) p is the hydrostatic pressure which cannot be determined from a knowledge of the deformation because of the assumption of material incompressibility, $\mathbf{1}$ is the unit matrix, σ_0 is the flow stress of the material of the rod in simple compression or tension and I is the second invariant of the strain-rate tensor $\mathbf{D}$. Equation (1) and the equation obtained by substituting eqn (3) into (2) are the field equations to be solved for $\mathbf{v}$ and p subject to a suitable set of boundary conditions. In terms of the non-dimensional variables

$$\bar{\mathbf{v}} = \mathbf{v}/v_0, \qquad \bar{\boldsymbol{\sigma}} = \boldsymbol{\sigma}/\sigma_0, \qquad \bar{p} = p/\sigma_0, \qquad \bar{r} = r/r_0, \qquad \bar{z} = z/r_0, \tag{6}$$

these field equations are

$$\operatorname{div} \mathbf{v} = 0, \tag{7}$$

$$-\operatorname{grad} p + \operatorname{div}((\operatorname{grad} \mathbf{v} + (\operatorname{grad} \mathbf{v})^T)/2\sqrt{3}\,I) = \alpha(\mathbf{v} \cdot \operatorname{grad})\mathbf{v} \tag{8}$$

where

$$\alpha = \rho v_0^2/\sigma_0 \tag{9}$$

is a non-dimensional number. In eqn (6), v_0 is the speed of the rod and r_0 its radius. In eqns (7) and (8) and hereafter the superimposed bars over the non-dimensional variables have been dropped. The operators grad and div in eqn (8) imply the gradient and divergence operators in terms of the non-dimensional coordinates. We note that there is only one non-dimensional number α that governs the steady state deformations of the rod.

For the boundary conditions on the rod/cavity interface, we assume that

$$\mathbf{t} \cdot (\boldsymbol{\sigma}\mathbf{n}) = 0, \tag{10}$$

$$\mathbf{v} \cdot \mathbf{n} = 0, \tag{11}$$

where $\mathbf{n}$ and $\mathbf{t}$ are, respectively, a unit normal and unit tangent vector on the interface. The boundary condition (10) represents smooth contact between the rod and target. This appears reasonable since a thin layer of material at the interface either melts or is severely degraded by adiabatic shear. The boundary conditon (11) represents no interpenetration of the rod material into the target and vice versa. On the free surface of the rod,

$$\boldsymbol{\sigma}\mathbf{n} = \mathbf{0}, \tag{12}$$

$$\mathbf{v} \cdot \mathbf{n} = 0, \tag{13}$$

where $\mathbf{n}$ is a unit outward normal to the surface. The boundary condition (13) implies that the velocity of particles on the surface is tangent to the surface. Out of the boundary conditions (12) and (13) only the former is needed to specify the boundary-value problem completely provided the shape of the free surface is known. Since such is not the case, we use eqn (13) to check whether the presumed free surface is correct or not. On the rod cross-section far from the cavity bottom

$$|\mathbf{v} + \mathbf{e}_z| \to 0 \quad \text{as} \quad z \to \infty, \tag{14}$$

and on the deformed rod material at the cavity outlet

$$|\boldsymbol{\sigma}\mathbf{n}| \to 0 \quad \text{as} \quad |r^2 + z^2|^{1/2} \to \infty. \tag{15}$$

Equation (14) implies that the end of the rod far from the bottom of the cavity is moving with a uniform velocity in the negative z-direction and eqn (15) is equivalent to the statement that the surface of the deformed rod near the cavity outlet is traction free. In order to state the problem more precisely one should specify the rates at which quantities indicated in eqns (14) and (15) decay. But at the present time there is little hope of establishing an existence and uniqueness theory for the problem and, therefore, specification of rates of decay in eqns (14) and (15) is not required. Here we seek an approximate solution of the problem numerically.

FINITE ELEMENT FORMULATION OF THE PROBLEM

To solve the problem numerically we usually consider a finite region. Thus the region of the deformable rod analyzed is shown in Fig. 1 wherein is also indicated its spatial discretization. We note that since the shape of the free surface is not known *a priori* we estimate one and will subsequently check whether or not it is an appropriate one. If not, we will modify the same and keep on iterating till a prespecified criterion is met. This is elaborated upon below. The boundary conditions (10)–(12), (14) and (15) are replaced by the following:

$$\sigma_{rz} = 0, \qquad v_r = 0 \text{ on the axis of symmetry AB}, \tag{16.1}$$

$$\mathbf{v} \cdot \mathbf{n} = 0 \text{ and } \mathbf{t} \cdot (\boldsymbol{\sigma}\mathbf{n}) = 0 \text{ on the cavity surface BC}, \tag{16.2}$$

$$\boldsymbol{\sigma}\mathbf{n} = \mathbf{0} \text{ on the free surface DEF}, \tag{16.3}$$

$$v_z = -1.0, \qquad v_r = 0 \text{ on AF}, \tag{16.4}$$

$$\mathbf{v} = v_e\mathbf{n} \text{ and } \mathbf{t} \cdot (\boldsymbol{\sigma}\mathbf{n}) = 0 \text{ on the outlet surface CD}. \tag{16.5}$$

As before $\mathbf{n}$ is a unit outward normal to a surface and $\mathbf{t}$ is a unit tangent to the surface. The boundary condition (16.5) implies that the rod particles at the exit surface CD are traveling normal to the surface with a uniform speed v_e and the tangential traction on it is zero. The value of v_e is computed by equating the amount of material flowing out through CD to that flowing in through AF. We now obtain a variational statement for the boundary value problem defined by eqns (7), (8) and (16).

Let $\boldsymbol{\phi}$ be a smooth vector valued function defined on the region R, shown enclosed by ABCDEF in Fig. 1, and $\phi_r = 0$ on AB, $\boldsymbol{\phi} \cdot \mathbf{n} = 0$ on BC, $\boldsymbol{\phi} = 0$ on AF and $\boldsymbol{\phi} \cdot \mathbf{n} = 0$ on CD. Also let ψ be a bounded scalar valued function defined on R. Multiplying both sides of eqn (7) with ψ, taking the scalar product of both sides of eqn (8) with $\boldsymbol{\phi}$, integrating the resulting equations on the domain R, using the divergence theorem, the traction boundary conditions in (16) and the above stated side conditions on $\boldsymbol{\phi}$ we arrive at the following.

$$\int_R \psi(\operatorname{div} \mathbf{v})\, \mathrm{d}V = 0, \tag{17.1}$$

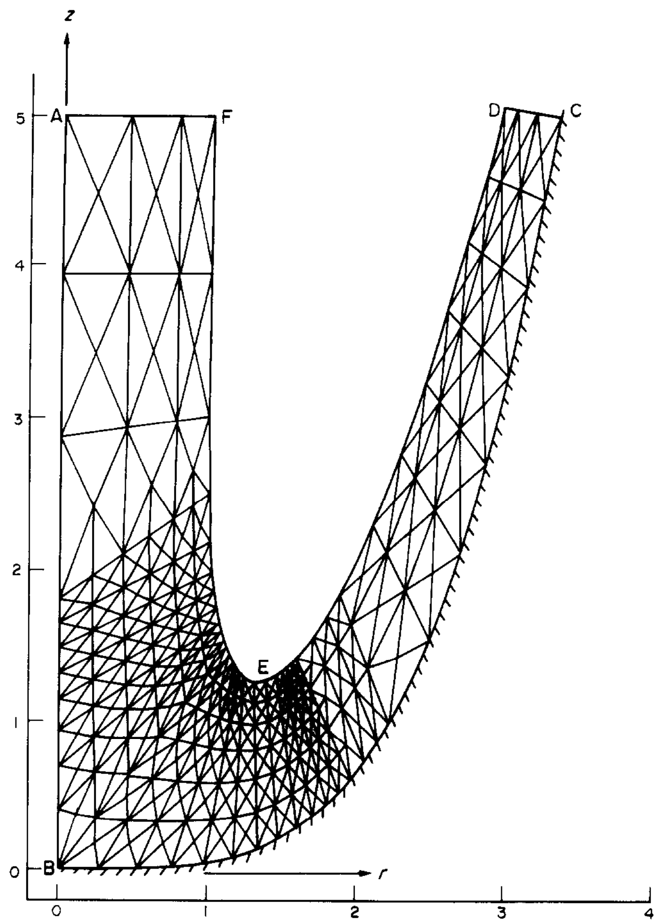

Fig. 1. The region studied and its finite element discretization.

$$\int_R p(\operatorname{div}\boldsymbol{\phi})\,\mathrm{d}V - \int_R \frac{1}{2\sqrt{3}\,I}\mathbf{D} : (\operatorname{grad}\boldsymbol{\phi} + (\operatorname{grad}\boldsymbol{\phi})^T)\,\mathrm{d}V = \alpha\int_R \{(\mathbf{v}\cdot\operatorname{grad})\mathbf{v}\}\cdot\boldsymbol{\phi}\,\mathrm{d}V. \quad (17.2)$$

Here a single dot implies the scalar product between two vectors and the symbol : stands for the scalar product between two second order symmetric tensors. Thus a weak formulation of the boundary-value problem given by eqns (7), (8) and (16) is to find p and $\mathbf{v}$ defined on R such that eqns (17) holds for every ψ and $\boldsymbol{\phi}$, ψ and grad $\boldsymbol{\phi}$ are square integrable over R, $\boldsymbol{\phi}$ satisfies the homogeneous essential boundary conditions stated above and $\mathbf{v}$ satisfies the essential boundary conditions outlined in eqns (16).

We refer the reader to Becker *et al.* [8] for details of obtaining a finite element solution of eqns (17). Suffice it to say that eqns (17) are solved by using the following iterative scheme.

$$\int_R \psi(\operatorname{div}\mathbf{v}^m)\,\mathrm{d}V = 0, \quad (18.1)$$

$$\int_R p^m(\operatorname{div}\boldsymbol{\phi})\,\mathrm{d}V - \int_R \frac{1}{2\sqrt{3}\,I^{m-1}}\mathbf{D}^m : (\operatorname{grad}\boldsymbol{\phi} + (\operatorname{grad}\boldsymbol{\phi})^T)\,\mathrm{d}V = \alpha\int_R \{(\mathbf{v}^{m-1}\cdot\operatorname{grad})\mathbf{v}^m\}\cdot\boldsymbol{\phi}\,\mathrm{d}V \quad (18.2)$$

Here m is the interation number. Note that the hydrostatic pressure p appears linearly and its previous values are not needed. The initial velocity field is taken to be zero for small values of α. If the solution is known for some α, it is taken as the initial solution when solving the problem for the next higher value of α. The iteration process in (18) is stopped if, at each nodal point,

$$\|\mathbf{v}^m - \mathbf{v}^{m-1}\| \leq 0.01\,\|\mathbf{v}^{m-1}\| \quad (19)$$

where $\|\mathbf{v}\|^2 = (v_r^2 + v_z^2)$. When the velocity field corresponding to $(\alpha - 1)$ was taken as the initial estimate for the solution to be computed for an assigned value of α, it took nearly 10 iterations for the convergence criterion (19) to be satisfied.

TREATMENT OF THE FREE SURFACE

In the preceding finite element formulation of the problem the shape of the free surface DEF was presumed to be given. Since it is not known *a priori* we presume one, solve the problem and then see if the condition (13) is satisfied on it or not. Improving upon the presumed shape of the free surface DEF if (13) is not satisfied required a considerable effort. We note that problems in which the shape of the free surface is to be determined as a part of the solution of the problem have been solved by Zienkiewicz *et al.*, [9], Oden and Lin [10], and Batra *et al.* [11]. For us the following technique proved quite effective.

Starting from the point F we found the parabolic curve passing through F and the next two nodes downstream from it. We then found the tangent to the curve and a unit normal $\mathbf{n}$ at the middle node. We evaluated the magnitude of the error

$$e \equiv \mathbf{v} \cdot \mathbf{n} / \|\mathbf{v}\| \tag{20}$$

at the middle node and repeated this procedure for all of the nodes. Note that the node F is fixed and the last node D on the free surface was assumed to be on the straight line passing through the two nodes immediately preceding to it on the free surface DEF. That is, the curvature of DE near the point D was presumed to be zero. Points where the magnitude of the error e was not smaller than a preassigned small number were moved along $\mathbf{n}$ or $-\mathbf{n}$ according as e was positive or negative and the distance moved was proportional to the magnitude of e. A check was made to ensure that two different nodes on the presumed free surface are not mapped into the same location when modifying the shape of the free surface. The procedure was repeated until the error e at each node on the free surface DEF was less than 0.1. It was found computationally very efficient to switch to the following method for adjusting the free surface subsequently. Let H and K be two successive nodes on the free surface downstream from G, $\mathbf{N}$ be the normal vector to the previously assumed free surface at K, $\mathbf{T}$ be a vector parallel to $\mathbf{v}$ computed at K and we wish to find the new location K′ of K. It is at the point of intersection K′ of $\mathbf{N}$ with the circular arc that passes through G and H, and has a tangent vector at K′ parallel to $\mathbf{T}$. This eliminates the likelihood of two nodes ending up at the same location during a refinement of the shape of the free surface. With this technique the magnitude of e at each node point on the surface DEF could be reduced to less than 5% and the average of $|e|$ for all nodes on DEF to less than 1.5% in at most six iterations.

COMPUTATION AND DISCUSSION OF RESULTS

The finite element program developed earlier [6] to solve the companion problem of a rigid rod penetrating into a deformable target was modified to study the present problem. It employs 6-noded triangular elements and within each element the velocity (pressure) field is approximated by a quadratic (linear) function defined in terms of its values at 6 (3 corner) nodes. Thus both the velocity and pressure fields are continuous across interelement boundaries. We note the element satisfies the Babuška–Brezzi [12] condition. The velocity boundary condition in (16.2) is accounted for by using the method of Lagrange multipliers. The sample problem used to establish the validity of the code has been discussed in [6].

In Fig. 2 is plotted the computed velocity field for $\alpha = 5.1$. The details of the velocity field within the vicinity of the point where the curvature of the free surface changes sharply are also shown. As is rather obvious from the plotted results the Lagrange multipler method is quite effective in satisfying the essential boundary condition (16.2) on the cavity surface. We note that on the computed free surface the velocity of points is along the tangent to the surface. All of the results presented herein are for a fixed shape of the cavity given by

$$z = 0.04r^4.$$

This shape of the cavity was chosen after several trials; the selection criterion being that the

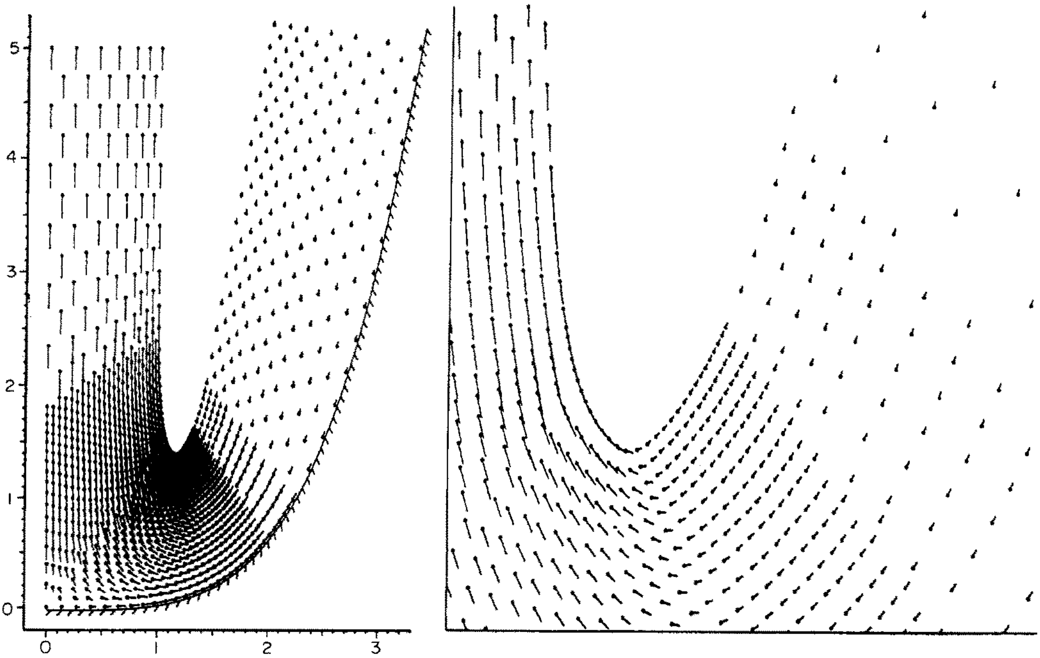

Fig. 2. The computed velocity field for $\alpha = 5.1$.

part of the surface over which the deformed rod particles exhibit a tendency to separate away from the surface BC is as small as possible. Ideally the contact should be maintained over all of BC but such a goal proved essentially impossible to attain especially for different striking speeds of the rod.

The velocity field for other values of α was quite similar to that shown in Fig. 2. As the speed of the rod increased the free surface moved away from the fixed cavity so that the thickness of the region at the outlet increased. The shapes of the free surface for different values of α are shown in Fig. 3. The radius of curvature near the bottom of the surface decreases sharply as the speed of the rod is increased. The plot of the thickness at the outlet versus α in Fig. 3 shows

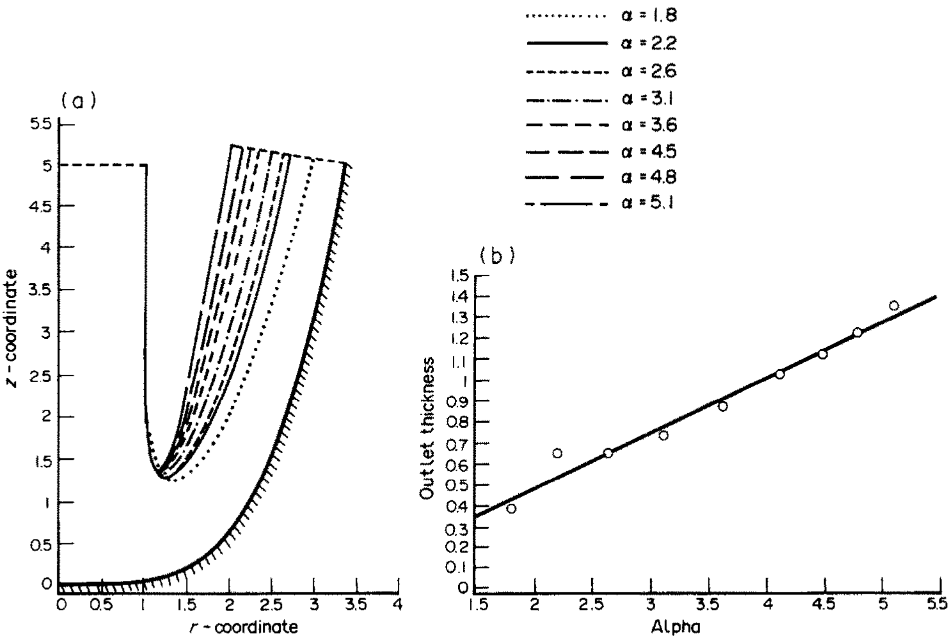

Fig. 3. a. Shapes of the free surface for different values of α. b. Thickness of the outlet region versus α.

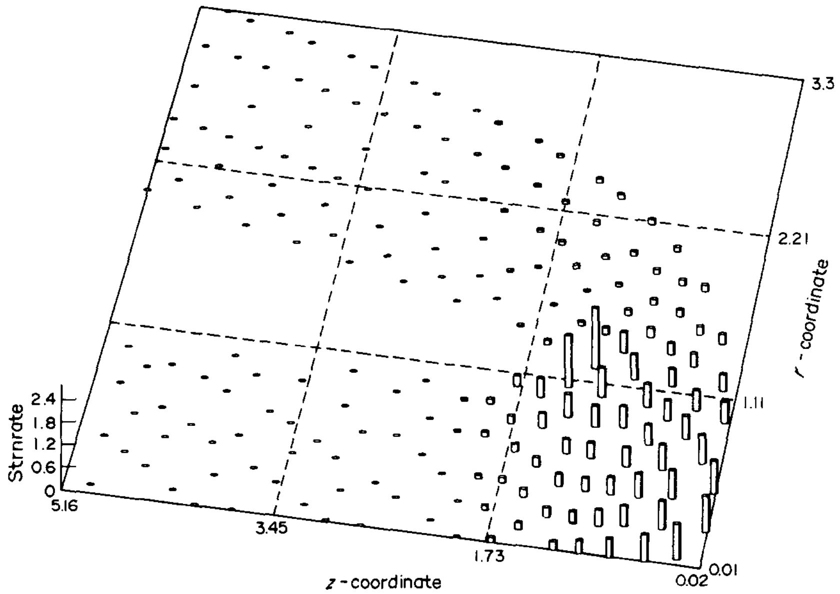

Fig. 4. Variation of the second invariant I of the stretching tensor $\mathbf{D}$ in the deforming region.

that the thickness increases linearly with α. Since the speed of the rod at the inlet is always taken to be 1.0, the speed of the particles at the outlet decreases so as to satisfy the balance of mass.

Figure 4 depicts the variation of the second invariant I of the strain-rate tensor $\mathbf{D}$ in the deforming region. As one would expect severe deformations take place in the region near the bottom of the cavity. Larger values of I occur near the bottom of the free surface where the flow reverses. For typical values of the radius of the penetrator these non-dimensional values of I are to be multiplied by 10^5 indicating thereby that peak strain-rates of the order of 10^5–$10^6\,\mathrm{s}^{-1}$ occur in the vicinity of the point on the free surface where the flow reverses. We note that the

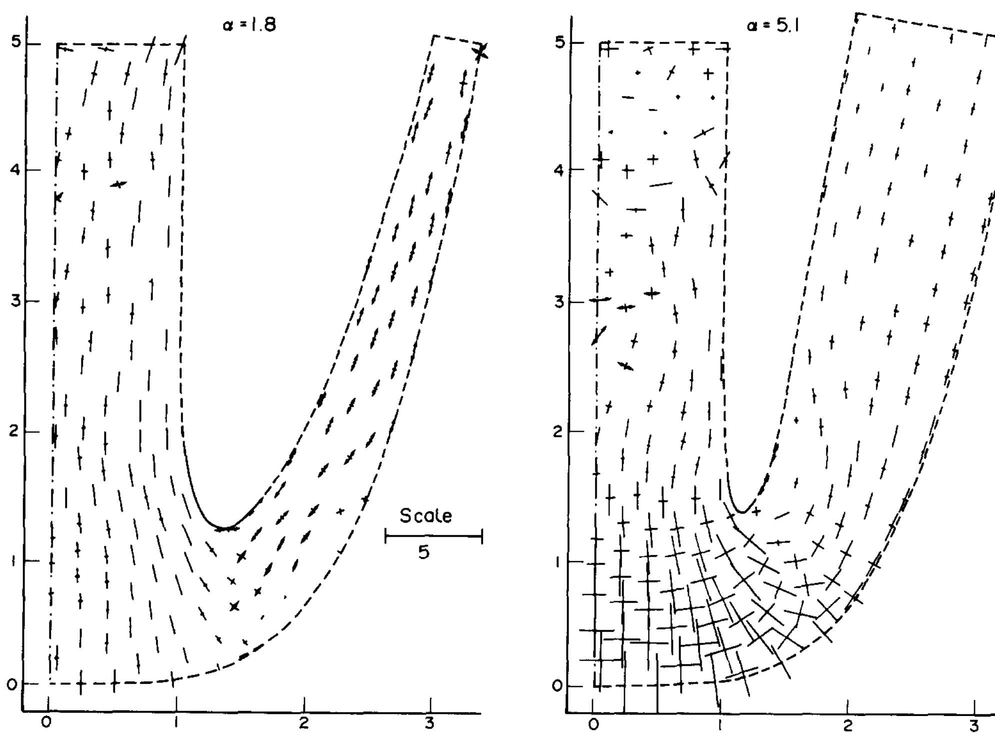

Fig. 5. Principal stresses in the deforming region.

non-dimensional values of I and their locations in the deforming region did not vary much with α. In Figs 5 and 6 are plotted, respectively, the principal stresses and the hydrostatic pressure in the deforming region for two different values of α. The lines are oriented along the axes of principal stresses and their lengths are proportional to the magnitudes of principal stresses at that point. The arrows at the ends of a line indicate that the corresponding principal stress is tensile otherwise it is compressive. Whereas for $\alpha = 1.8$ the material particles whose velocity in the z-direction is opposite to that of the incoming rod experience tensile stresses such is not the case at the higher value of α. This transition seems to take place around $\alpha = 3.6$. For $\alpha = 1.8$ one of the principal stresses at points in the region between the free surface and the bottom of the cavity is compressive; the other one is essentially zero. At the higher value of α both principal stresses are compressive. This is possibly due to the increase in the hydrostatic pressure (cf. Fig. 6) with the speed of the rod. Since the strain rates at points near the inlet and the outlet surface are negligibly small, and the values of stresses at these points, as given by

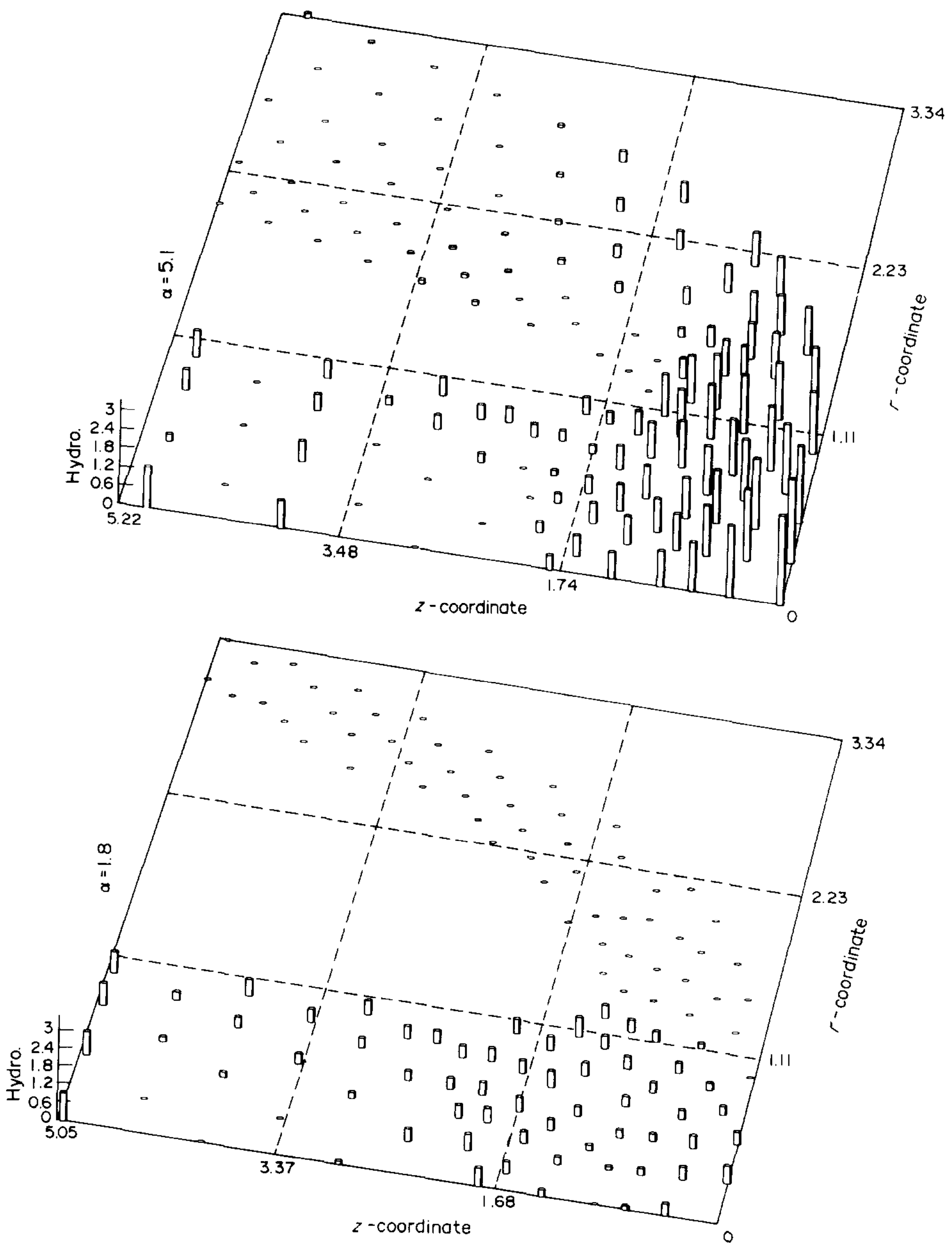

Fig. 6. Distribution of the hydrostatic pressure p in the deforming region.

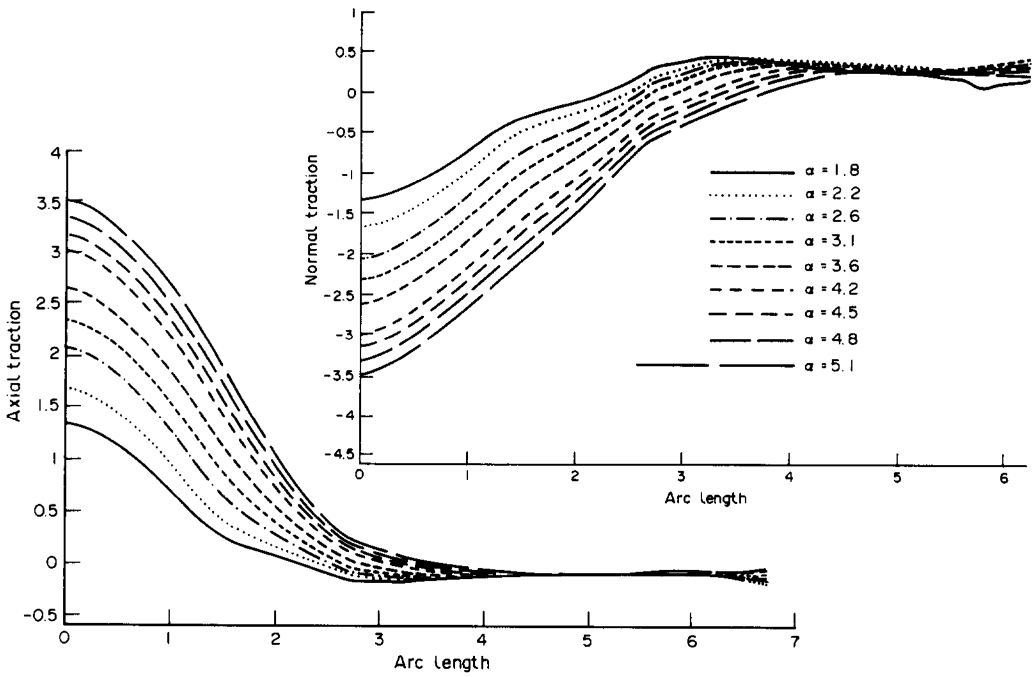

Fig. 7. Variation of the normal and axial tractions on the cavity wall.

eqn (3), are computed by taking the ratio of two small numbers, the magnitudes of stresses at these points may not be very accurate. This is one possible explanation for the small tensile stresses at points near the inlet and outlet surfaces. At a few isolated points in the vicinity of the bounding surfaces near the inlet and outlet regions the computed values of the hydrostatic pressure were relatively small negative numbers.

There is a tendency for the material particles to leave the cavity wall near the outlet region. This is indicated by the negative values of the computed normal traction at these points. The normal tractions and the axial tractions at different points on the cavity wall are plotted in Fig. 7. The arc length along the cavity surface is measured from the point of intersection of the cavity and the axis of the rod. For the same cavity surface the point where separation tends to occur moves away from the centroidal axis of the rod as the speed of the rod is increased. We note that in our computations material particles were not allowed to leave the cavity surface. Since the magnitude of the normal tractions at these points is rather small and the distance of these points from the center of the rod is of the order of $2r_0$, the computed results especially in the severely deformed region near the bottom of the cavity are quite meaningful. It is now obvious that to keep, say, the horizontal distance of the point on the cavity wall where separation tends to occur from the centroidal axis of the rod constant, the shape of the cavity should be adjusted as the rod speed is varied. The axial traction plotted in Fig. 7 indicates that the contribution to the total axial force from points where flow separation would have occurred is very small. This is due to the fact that the angle between the cavity surface at these points and the axis of the rod is very small so that the normal to the cavity surface at these points is essentially perpendicular to the rod axis.

How the total axial force acting on the cavity surface and experienced by the rod depends upon α is shown in Fig. 8. Unlike the case of a rigid rod penetrating into a rigid/perfectly plastic target where the axial force acting on the penetrator depended weakly on the penetrator speed, here the dependence of the axial force upon α is rather strong. We note that whereas herein the calculations have been performed with one cavity surface, in the actual penetration problem the surface separating the deforming penetrator and target regions will alter with the speed of the penetrator when all other parameters are kept fixed. In the approximate theory of Tate [13] the axial force acting at the penetrator/target interface is presumed to be constant. We have not investigated the dependence of the axial force upon the shape of the assumed cavity. Since there is very little experimental data available in the open literature it is hard to

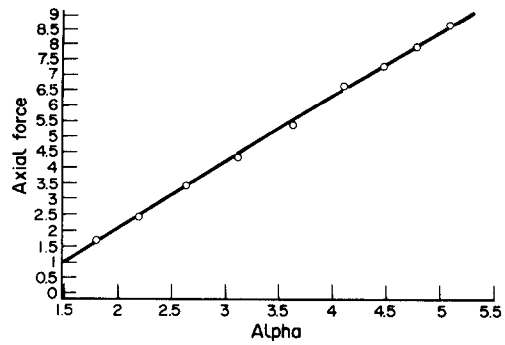

Fig. 8. Dependence of the total axial force acting on the cavity wall upon α.

judge whether or not the cavity surface envisaged here is close to those observed experimentally.

We note that strain-rates and therefore the rod deformations are negligibly small near the inlet and outlet regions. This ensures that the assumed finite region considered for solving the problem numerically is sufficient. The computed solution seemed to be stable in the sense that either superimposed small perturbations died out to zero or following slightly different paths gave the same solution.

CONCLUSIONS

For the fixed cavity the thickness at the outlet increases linearly with α, and the total axial force acting on the cavity wall depends strongly upon α. Most severe deformations occur in the region near the cavity bottom and the point where the curvature of the free surface changes. Peak strain-rates in the range 10^5–$10^6\,s^{-1}$ invariably occurred at or near the bottom E (Fig. 1) of the free surface. The hydrostatic pressure increases considerably with α. Whereas at lower speeds of the rod tensile stresses developed at points on the exist side of the flow these were overcome by the increase in the value of the hydrostatic pressure at higher speeds of the rod. The point on the cavity wall where the flow had a tendency to separate from the wall moved away from the axis of the rod as the striking speed increased.

Acknowledgement—This work was supported by the U.S. Army Research Office Contract DAAG 29-85-K-0238 to the University of Missouri-Rolla.

REFERENCES

[1] T. W. WRIGHT, A survey of penetration mechanics for long rods. In *Lecture Notes in Engineering*, Vol. 3, Computational Aspects of Penetration Mechanics (Edited by J. Chandra and J. Flaherty). Springer-Verlag, New York (1983).
[2] M. E. BACKMAN and W. GOLDSMITH, *Int. J. Engng Sci.* **16**, 1 (1978).
[3] G. H. JONAS, and J. A. ZUKAS, *Int. J. Engng Sci.* **16**, 879 (1978).
[4] C. E. ANDERSON JR and S. R. BODNER, *Third TACOM Armor Coordinating Conference*, Monterey, Calif. (1987).
[5] M. RAVID and S. R. BODNER, *Int. J. Engng Sci.* **21**, 577 (1983).
[6] R. C. BATRA and T. W. WRIGHT, *Int. J. Engng, Sci.* **24**, 41 (1986).
[7] W. PRAGER and P. HODGE, *Theory of Perfectly Plastic Solids*. Dover, New York (1968).
[8] E. BECKER, G. CAREY and J. T. ODEN, *Finite Elements—An Introduction*, Vol. 1. Prentice-Hall, Englewood Cliffs, N.J. (1981).
[9] O. C. ZIENKIEWICZ, E. ONATE and J. C. HEINRICH, *Int. J. Numer. Meths Engng* **17**, 1497 (1981).
[10] J. T. ODEN and T. L. LIN, *Comp. Meth. Appl. Mechs. Engng* **57**, 297 (1986).
[11] R. C. BATRA, M. LEVINSON and E. BETZ, *Int. J. Numer. Meths Engng* **10**, 767 (1976).
[12] G. J. CAREY and J. T. ODEN, *Finite Elements—A Second Course*, Vol. 2. Prentice Hall, Englewood Cliffs, N.J. (1983).
[13] A. TATE, *J. Mechs. Phys. Solids* **15**, 387 (1967); *ibid*, **17**, 141 (1969).

(*Received* 30 *June* 1987)